Linking Statistical and Hydrodynamic Modeling for Compound Flood Hazard Assessment in Tidal Channels and Estuaries

Hamed Moftakhari[1,2], Jochen E Schubert[1], Amir AghaKouchak[1], Richard Matthew[1], Brett F Sanders*[,1]

1   University of California, Irvine
2   The University of Alabama

*Corresponding author: bsanders@uci.edu

Keywords:
Coastal Flood Hazards, Bivariate Statistical Analysis, Hydrodynamic Modeling, Compound Flooding

Highlights
- Compound flood hazard levels computed for tidal channels or estuaries.
- Bivariate statistical and hydrodynamic modeling is linked.
- Spatially distributed flood hazard levels computed for return period T.
- Method accounts for statistical and physical compounding effects.

Abstract

A method to link bivariate statistical analysis and hydrodynamic modeling for flood hazard estimation in tidal channels and estuaries is presented and discussed for the general case where flood hazards are linked to upstream riverine discharge Q and downstream ocean level, H. Using a bivariate approach, there are many possible combinations of Q and H that jointly reflect a specific return period, T, raising questions about the best choice as boundary forcing in a hydrodynamic model. We show, first of all, how possible Q and H values depend on whether the definition of T corresponds to the probability of exceedance of "H OR Q" or "H AND Q". We also show that flood hazards defined by "OR" return periods are more conservative than "AND" return periods. Finally, we introduce a new composite water surface profile to represent the spatially distributed hazard for return period T. The composite profile synthesizes hydrodynamic model results from the "AND" hazard scenario and two scenarios based on traditional univariate analysis, a "Marginal Q" scenario and a "Marginal H" scenario.
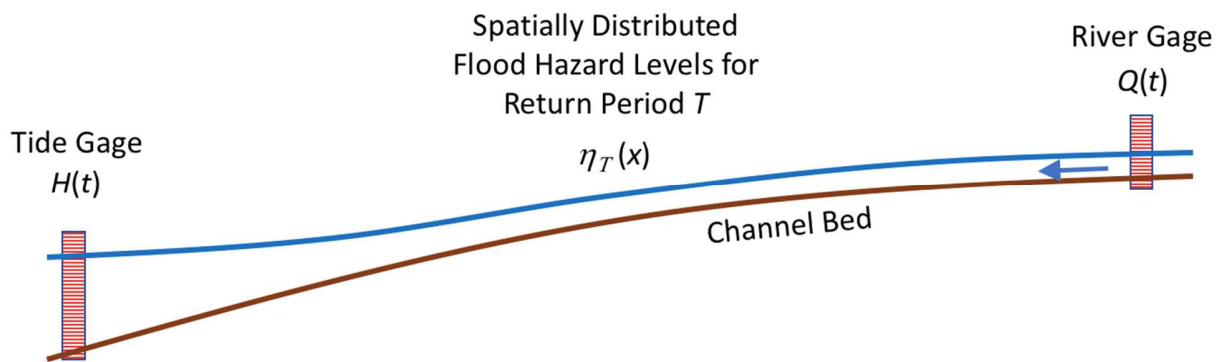
1. Introduction:

Flood risk is increasing in coastal cities around the world due to several factors including population growth, economic development, sea level rise, subsidence, land use changes and intensification of rainfall (Hallegatte et al., 2013; Hanson et al., 2011). By the year 2100, between 0.2–4.6% of global population and 0.3–9.3% of global gross domestic product may be exposed to coastal flooding if no adaptation occurs (Hinkel et al., 2014).

Management of flood risk relies on statistical and hydrodynamic modeling to delineate populations and assets exposed to flooding, anticipate and monetize the consequences of flooding, and develop cost effective and socially robust interventions including infrastructure projects, insurance programs, land use and building code policy changes and emergency preparedness and response measures (Sayers et al., 2013, Luke et al. 2018). To address risks, statistical and hydrodynamic modeling is linked to delineate spatial fields of the intensity of flooding (e.g., depth and velocity) for a set of exceedance probabilities, information which is subsequently used to estimate average annual losses based on exposed assets and their vulnerability to damage (Scawthorn et al., 2006). The linking of statistical and hydrodynamic modeling is straightforward when addressing a single hazard such as river discharge, Q. Flood risk is modeled by first performing univariate frequency analysis of annual maximum discharge to estimate extreme values $\hat{Q}_T$ for yearly return periods T (e.g., $\hat{Q}_{100}$ for 100 year return period discharge). Here, the hat notation indicates annual maximum discharge and the subscript refers to the return period. Second, hydrodynamic modeling is performed with $\hat{Q}_T$ as a boundary condition to characterize spatial fields of water surface elevation at each return period, $\eta_T(x)$, where x represents distance along the river (FEMA, 2018). However, coastal hazard assessment must account for interaction of river flooding, intense rainfall, storm surge and waves and the likelihood of a coincidence in extreme and non-extreme levels of these hazards which is also known as compounding effects

65 (Gallien et al., 2018; Moftakhari et al., 2017). One of the most important
66 compounding effects is the interaction of river discharge and the downstream ocean
67 level, H, in tidal channels and estuaries. Of the world's 32 largest cities, 22 are
68 located on estuaries (Ross, 1995), at which the interactions between Q and H play a
69 major role in flood risk estimation (Ward et al., 2018). In the U.S. alone, 140 million
70 people (~50% of total population) live on the coast in close proximity to an estuary
71 (Kennish, 2004).

Spatially Distributed Flood Hazard Levels for Return Period T

River Gage $Q(t)$

Tide Gage $H(t)$

$\eta_T(x)$

Channel Bed

72

73 **Figure 1:** The spatial distribution of the T-year return period extreme water level, $\eta_T(x)$, in an estuary or tidal
74 channel (blue line) depends on upstream river discharge $Q(t)$, downstream ocean water levels $H(t)$, and the
75 system geometry and resistance to flow. This paper shows how bivariate statistical analysis and
76 hydrodynamic modeling can be linked to compute $\eta_T(x)$.

77

78   Figure 1 illustrates the estuarine flood hazard problem: the objective is to
79 estimate spatially distributed extreme water levels, $\eta_T(x)$, for return period T in a
80 tidal channel or estuary. We assume knowledge of the system geometry (e.g., bed
81 elevation, channel width and shape) and resistance to flow (e.g., Manning resistance
82 coefficient). We also assume that gauges provide time series records of boundary
83 conditions: river discharge measurements representative of what enters the reach,
84 $Q(t)$, and water level measurements, $H(t)$, representative of the downstream end of
85 the reach. Hence, the key question becomes: how can statistical and hydrodynamic
86 modeling be linked for the estuarine setting involving two gage records
87 characterizing two different aspects of hydrodynamic extremes? Put another way,
88 can the existing paradigm of univariate flood hazard modeling described above for

89   rivers be extended to account for a second gage in a relatively simple and
90   straightforward way? We write this mathematically as follows,

$$\eta_T(x) = f\big(Q(t), H(t), p(x)\big) \qquad [1]$$

92   where $p(x)$ represents the parameters describing the channel geometry and
93   resistance properties. Note that Eq. [1] can be extended for two-dimensional flood
94   hazard levels by interpreting x as two-dimensional vector representing geographical
95   coordinates.

96   In the absence of robust models for extreme water levels in estuaries, overly
97   simplistic bathtub models have received widespread use for estimating coastal
98   flooding hazards and the resulting human exposure at regional (Torresan et al.,
99   2012) and national/international levels (Dasgupta et al., 2011; Hinkel et al., 2010).
100   Bathtub models simply take an estimated extreme water level and extrapolate it
101   inland to estimate population and assets exposed to flooding, which neglects the
102   potential for flood stage to change with distance inland as a consequence of riverine
103   forcing and/or tidal damping/amplification (Lanzoni and Seminara, 1998). This
104   points to the potential for underestimation of flood consequences. On the other
105   hand, bathtub models may also overestimate flood consequences by failing to
106   account for flood defenses and the role of friction, inertia and storage in flooding
107   dynamics (Gallien et al., 2014; Sanders, 2017). With the integration of statistical and
108   hydrodynamic models to estimate extreme water levels, more robust estimates of
109   extreme water levels become possible as well as mechanistic routing of flood water
110   into adjacent urban areas to estimate flood impacts (Gallien et al., 2014, 2011).

111   Existing methods for flood hazard assessment (solving Eq. 1) in tidal
112   channels are limited (Hoitink and Jay, 2016). In particular, for the case where $\hat{Q}_T$
113   and $\hat{H}_T$ are statistically independent, FEMA (2015) recommends the following
114   procedure to estimate the hazard for return period T: (1) univariate analysis of
115   annual maximum river discharge to estimate $\hat{Q}_T$ and univariate analysis of annual
116   maximum total water level to estimate $\hat{H}_T$, (2) a pair of hydrodynamic model

117   simulations with one forced by $\hat{Q}_T$ and a non-extreme H value (usually chosen as

118   mean higher high water) and the other forced by $\hat{H}_T$ and a non-extreme Q value, and

119   (3) synthesis of the two hydrodynamic model simulations based on the pointwise

120   maximum water level across the two simulations. An appealing aspect of the FEMA

121   approach is that only two hydrodynamic simulations are required for each return

122   period, which is important because resources for flood mapping are limited (Burby,

123   2001) and because hydrodynamic flood simulation is computationally demanding

124   (i.e., many hours for one simulation) especially for urban areas where fine

125   resolution grids are needed to accurately depict flooding, e.g., Gallien et al. (2014,

126   2011). Hence, the FEMA (2015) approach is aligned with needs for simple and

127   efficient assessment approaches. Nevertheless, there are significant limitations. For

128   example, univariate statistical analysis is not appropriate when $\hat{Q}_T$ and $\hat{H}_T$ exhibit

129   statistical dependence also known as compound risks (Leonard et al., 2014;

130   Moftakhari et al., 2017; Zscheischler et al., 2018). Additionally, even when $\hat{Q}_T$ and

131    $\hat{H}_T$ are independent, extreme water levels may occur over the length of the tidal

132   reach due to the interaction of non-extreme boundary forcing values. FEMA (2018,

133   2015) does not presently offer guidance to address this situation. Broadly, the FEMA

134   (2015) guidance is recommends multi-hazard assessment based on the

135   predominant hazards, yet limitations of this approach are increasingly being

136   recognized (Hillier et al. 2015).

137   The aforementioned challenges of linking statistical and hydrodynamic

138   modeling can only be partly overcome with improved access to, and reduced costs

139   of, high performance computing systems that map flood hazards through Monte

140   Carlo simulation. That is, Monte Carlo simulation can be applied to depict thousands

141   of scenarios based on different combinations of $\hat{Q}_T$ and $\hat{H}_T$, and depict flood hazards

142   based on the frequency of the pointwise exceedance of a water level thresholds

143   (Purvis et al., 2008). However, bivariate statistical analysis is needed in place of

144   univariate analysis to properly describe the correlation structure of the hazard

drivers and for sampling representative combinations of hazard drivers in Monte Carlo simulations.

The objective of this paper is to present a solution method for Eq. 1 that accounts for statistical correlation structure and physical compounding effects (e.g., backwater) between boundary forcing values $\hat{Q}_T$ and $\hat{H}_T$ while using only a small number of hydrodynamic model simulations. Building on the existing methodology recommended by FEMA (2015), we present a four-step method as follows:

(1) Bivariate statistical analysis of Q and H records to yield possible $(\hat{Q}_T, \hat{H}_T)$ pairs for return period, T.

(2) Selection of N specific $(\hat{Q}_T, \hat{H}_T)$ pairs for hydrodynamic modeling. Here, we recommend N=4 (more detail will follow) although other options are possible.

(3) Hydrodynamic modeling of N scenarios defined by $(\hat{Q}_T, \hat{H}_T)$ pairs identified in Step 1 to yield spatial distributions of extreme water levels, $\eta_T^i(x)$, i=1, … ,N. Note that the subscript on η references return period and the superscript references the scenario.

(4) Synthesis of hydrodynamic modeling results, $\eta_T^i(x), i = 1, …, N$, to yield $\eta_T(x)$.

The remainder of the paper presents this method in detail along with applications. Section 2 presents methods and materials including data used in this study, the bivariate statistical analysis methods to determine all possible $(\hat{Q}_T, \hat{H}_T)$ pairs, identification of four specific pairs useful for hydrodynamic modeling, and methods for one-dimensional steady flow analysis and two-dimensional unsteady analysis of extreme water levels. Section 3 presents results of one-dimensional steady-flow analysis from several sites showing differences in water level profiles arising from the $(\hat{Q}_T, \hat{H}_T)$ pairs, and results of two-dimensional unsteady analysis at a single site where we further examine the limitations of the 1D

172 modeling and the added benefits of 2D modeling for assessment of coastal flood

173 hazards. Here, we also introduce an extension of the FEMA (2015) method that

174 offers potential to systematically improve the assessment of coastal flood hazards

175 by linking bivariate statistical analysis and hydrodynamic modeling. We close the

176 paper with discussion (Section 5) and conclusions (Section 6).

177 Broadly, this work shows that extending the univariate paradigm of river

178 flood hazard assessment to a bivariate paradigm of coastal flood hazard assessment

179 is not straightforward, as has been reported for many other types of compound

180 hazard (Kappes et al. 2012). Nevertheless, a systematic approach is possible and

181 shown herein. Furthermore, results point to the possibility that the existing FEMA

182 approach underestimates flood hazards where compounding effects are strong, and

183 we present a simple method to make a better estimate.

184

2. Methods and Materials

2.1. Data

Analysis herein focuses on tidal channels/estuaries in southern California (See Figure 2) where flood hazards are affected by extreme ocean levels and flood discharges: the Los Angeles River (LAR), the Santa Ana River (SAR) and Newport Bay (NB). For ocean level analysis, hourly ocean water level measurements were obtained from the National Oceanic and Atmospheric Administration (NOAA) Los Angeles tide gauge (gauge ID: 9410660) at hourly intervals. Tide gauge measurements capture water level fluctuations from combined effects of tides, storm surge and other factors that affect sea levels on hourly and longer time scales, a reading that is sometimes called Total Water Level (TWL). Discharge measurements for the LAR were obtained from Los Angeles County Department of Public Works (LADPW) Station F319-R (LAR at Wardlow Road) and consisted of 92 years of annual maximum discharge data between 1928-2014. Discharge measurements for the SAR were obtained from USGS Gauge 11078000 (Santa Ana River at Santa Ana) and consisted of 94 years of annual maximum discharge data between 1923 and 2017. River discharge measurements for Newport Bay were obtained from the Orange County Department of Water Resources (OCDWR) Gauge 226 (San Diego Creek at Campus Drive) and consists of 39 years of instantaneous discharge (1978-2016). The San Gabriel River and Coyote Creek (see Figure 2) are not considered in this study since bivariate statistical analysis (see Section 3.1) showed no correlation between $\hat{Q}$ and $\hat{H}$ likely because of strong flow regulation from Whittier Narrows Dam located approximately 30 km from the coastline.

Topographic and bathymetric data for LAR, and SAR were taken from the 1 m resolution 2014 US Army Corps of Engineers National Coastal Mapping Program Topobathy Lidar DEM. Topographic and Bathymetric data for NB were based a DEM reported by Gallien et al. (2011) which merged several sources of topographic and bathymetric data.

213
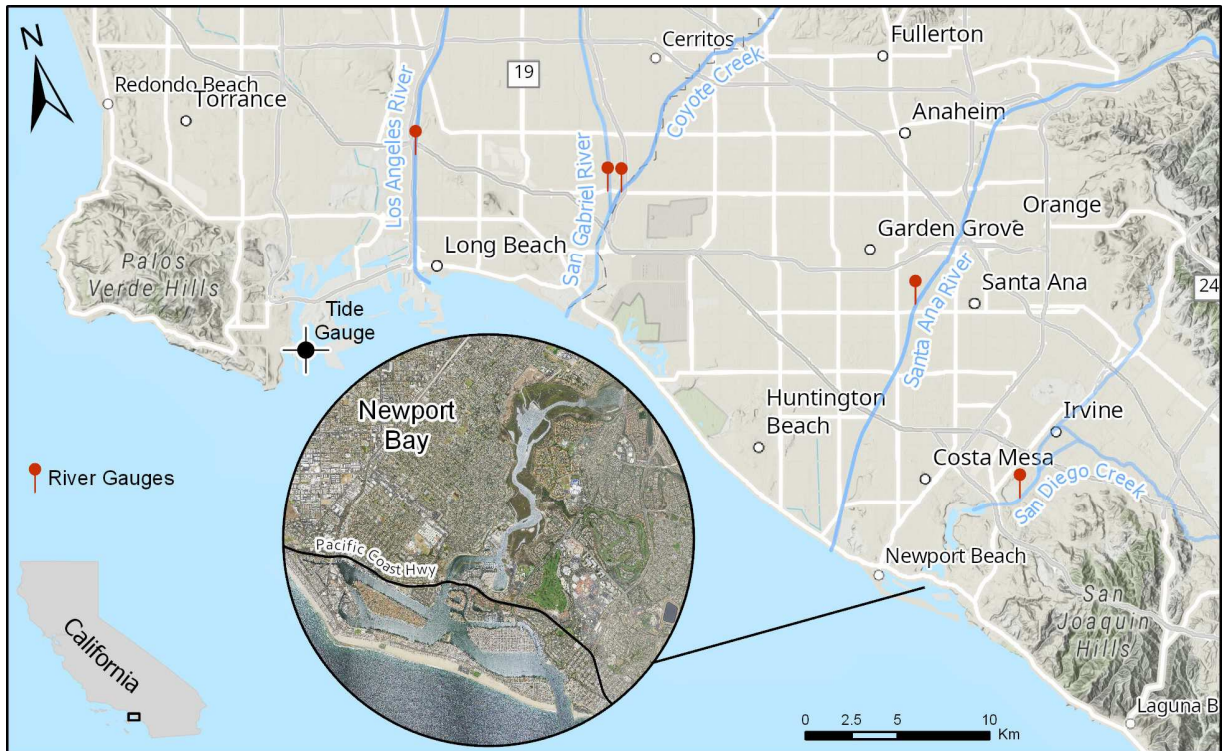
Figure 2: Compound flood hazards in southern California were examined for Los Angeles River, San Gabriel River, Santa Ana River, and Newport Bay using river discharge and ocean water level measurements at the gage locations shown.

2.2. Bivariate Statistical Analysis

Statistical analysis of extreme values of discharge and water level impacting a tidal reach or estuary are based on records of annual maximum values, although threshold-based approaches are also possible. Henceforth, we use a hat notation to indicate annual maxima data from the records of upstream discharge and downstream water level, $\hat{Q}$ and $\hat{H}$, respectively. Record lengths of several decades or more are preferred to enable estimation of water levels at relatively low frequencies, to be used for the design of infrastructure (e.g., return periods of 50 years or greater).

Bivariate statistical analysis begins with a test for correlation structure. While either linear or rank correlation coefficient measures can be used to assess the significance of the dependence between variables, tail dependence measures are

important for summarizing how extremes tend to occur simultaneously (Coles et al., 1999; Hao and Singh, 2016). Here, we employ joint density approaches over other alternatives (Hawkes et al., 2002; Heffernan and Tawn, 2004; Neal et al., 2013; Zheng et al., 2015) due to their flexibility, and computational/mathematical benefits (Hawkes, 2006; Salvadori et al., 2015).

According to Sklar's Theorem (Sklar, 1959), there exists a bivariate Copula function $C_{\hat{Q}\hat{H}}: [0,1] \times [0,1] \rightarrow [0,1]$ that formulates the joint distribution $F_{\hat{Q}\hat{H}}$ of the pair $(\hat{Q}, \hat{H})$, with marginal distributions $F_{\hat{Q}}$ and $F_{\hat{H}}$, for all $(Q, H) \in R^2$, as:

$$F_{\hat{Q}\hat{H}}(Q,H) = C_{\hat{Q}\hat{H}}\left(F_{\hat{Q}}(Q), F_{\hat{H}}(H)\right) \qquad [2]$$

The multivariate model is constructed by fitting suitable univariate laws on the marginals, and an appropriate copula on the observed pairs (Genest and Favre, 2007; Salvadori et al., 2007). Here, we use the method of Sadegh et al. (2018) which comprehensively analyzes the dependence structure of multiple drivers of flooding, and models them using copula functions to estimate return design values and their underlying uncertainties (Sadegh et al., 2018). This approach first selects a marginal distribution from 17 univariate distributions based on measures of goodness-of-fit including Akaike Information Criterion (AIC) and Bayesian Information Criterion (BIC), and then chooses a copula model from 26 copula functions. Copula model parameters are inferred through a Bayesian inference approach with Markov Chain Monte Carlo (Sadegh et al., 2018, 2017). The joint probability can refer to the exceedance of $\hat{Q}$ AND $\hat{H}$ or the exceedance of $\hat{Q}$ OR $\hat{H}$ (Salvadori et al. 2016), and a case can be made for the relevance of both to coastal flood hazard assessment. First of all, risk assessment should reflect the possibility that flooding is caused by either extreme river discharge or extreme ocean levels, which is consistent with the OR scenario. On the other hand, hydrodynamic modeling involves the simultaneous occurrence of an upstream discharge and downstream water level, consistent with the AND scenario.

256   Newport Bay data are used to illustrate this process. Figure 3 presents the

257   outcome of bivariate statistical analysis using both the OR and the AND hazard

258   scenarios using the method of Sadegh et al. (2018). There is no statistically

259   significant correlation between river flow and ocean water level at Newport Bay, but

260   correlation was found between river flow and non-tidal residual (NTR) defined as

261   the difference between TWL and the astronomical tide level. Hence, bivariate

262   statistical analysis that takes correlation structure into account is presented here

263   using river flow and NTR. Figure 3 illustrates the similarities and differences

264   between univariate and bivariate statistical analysis as well as the relative

265   complexity introduced by the copula based AND and OR hazard scenarios. In

266   particular, Figure 3 shows plots of the marginal distributions of NTR (Fig. 3a) and

267   river flow (Fig. 3c) representative of what has traditionally been used for univariate

268   flood hazard assessment, while Fig. 3b shows the copula-based AND and OR hazard

269   scenarios. The AND and OR hazard scenarios are shown as iso- return period curve

270   for T=50 year within a two-dimensional space whereby every point corresponds to

271   a possible $(\hat{Q}_T, \hat{H}_T)$ pair for use in hydrodynamic modeling. Additionally, along each

272   iso- return period curve, there is a point of maximum probability density which

273   represents the most likely $(\hat{Q}_T, \hat{H}_T)$ pairs given the correlation structure. Note that

274   the most likely $(\hat{Q}_T, \hat{H}_T)$ pair for the OR hazard scenario exceeds extreme values

275   given by the marginal distributions, while the most likely $(\hat{Q}_T, \hat{H}_T)$ pair for the AND

276   hazard scenario falls below the values given by the marginal distributions. This

277   shows that the OR hazard scenario will lead to boundary forcing that is more

278   conservative (meaning a more cautious approach to risk management perspective)

279   than the AND hazard scenario.

280   Given theoretical characteristics of the OR iso-return period curves (Salvadori

281   et al., 2016) boundary forcing associated with $(\hat{Q}_T, \hat{H}_T)$ pairs at the ends of the OR

282   curve may far exceed values given by the marginal distributions for the same return

283   period. This shows that the OR scenario creates seemingly unrealistic (highly

284   conservative) hazard scenarios in areas of low probability density.

285
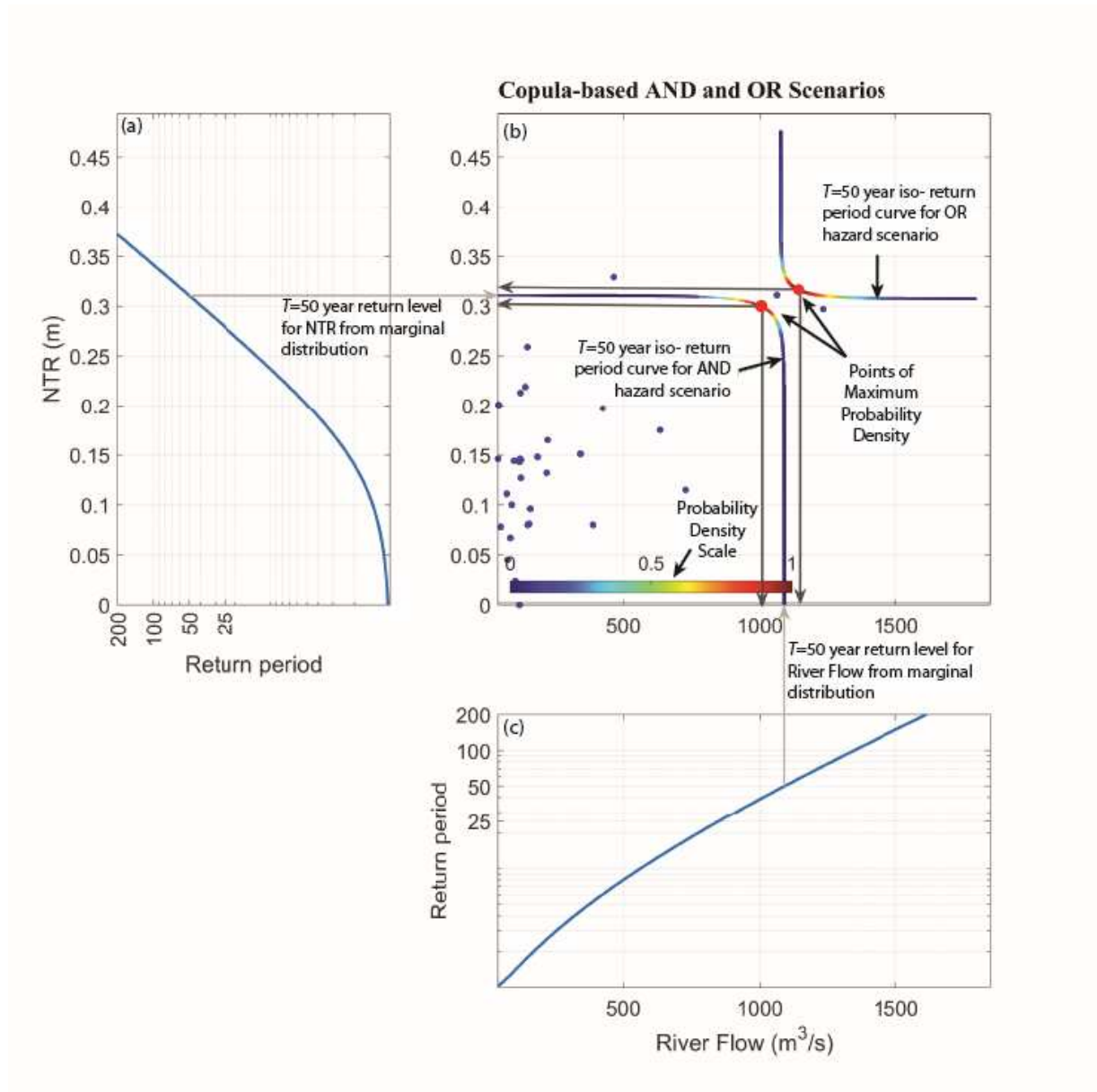
Figure 3: Marginal probability distribution for (a) non-tidal residual (NTR) which is a surrogate for $\hat{H}$ and (c)
River Flow $\hat{Q}$; (b) bivariate statistical analysis of $(\hat{Q}_T, \hat{H}_T)$ pairs based on copula-based AND and OR hazard
scenarios. Two iso- return period curves corresponding to T=50 year are shown. Note that ends of the copula-
based scenario curves for return period T are aligned with the return level of the marginal distribution for
return period T. Note also that along each T=50 year curve, there is a point of maximum probability density
which (due to correlation structure) represents the most likely $(\hat{Q}_T, \hat{H}_T)$ pairs. The most likely $(\hat{Q}_T, \hat{H}_T)$ pair

293 for the OR hazard scenario exceeds extreme values given by the marginal distributions, while the most likely

294 $(\hat{Q}_T, \hat{H}_T)$ pair for the AND hazard scenario falls below the values given by the marginal distributions.

295

296   Hydrodynamic modeling of compound flood hazards for return period T is

297 proposed based on four specific $(\hat{Q}_T, \hat{H}_T)$ pairs taken from bivariate statistical

298 analysis as shown in Figure 3:

299   (S1)   A "Marginal Q" scenario defined by the T-year return period river

300   discharge and a non-extreme water level downstream (typically taken

301   as mean higher high water).

302   (S2)   A "Marginal H" scenario defined by the T-year return period ocean

303   water level and a non-extreme river flow (typically taken as the daily

304   average flow).

305   (S3)   An "AND" scenario based on the $(\hat{Q}_T, \hat{H}_T)$ pair with the highest

306   probability density along the AND iso-return period curve.

307   (S4)   An "OR" scenario based on the $(\hat{Q}_T, \hat{H}_T)$ pair with the highest

308   probability density along the OR iso-return period curve.

309

310 FEMA (2015) presently recommends hydrodynamic modeling of S1 and S2 and

311 estimation of $\eta_T(x)$ based on the maximum of the two. Hence, two additional

312 scenarios (S3 and S4) are considered here as a way of leveraging bivariate statistical

313 analysis.

314

315   2.3.   Hydrodynamic Modeling

316   Dynamic changes in water surface elevation within estuaries can be

317 modeled with reasonable accuracy using shallow-water hydrodynamic models that

318 assume a constant fluid density and a depth-averaged horizontal velocity (FEMA,

319 2018, 2015; Sanders et al., 2010). Estuaries involve the mixing of riverine and ocean

320 water with different densities, and may be characterized by strong vertical density

321   stratification that acts as a major control on the velocity distribution and transport

322   (Geyer, 2010; Monismith, 2010). Consequently, three-dimensional models that

323   account for variable density from salinity and temperature are often needed to

324   estimate velocity distributions (Jay, 2010). However, the expression of density

325   effects on surface water elevation is weak and can be neglected when predicting

326   extreme water levels for the purpose of flood hazard modeling (Friedrichs, 2010). In

327   this study, water levels are modeled by solving one-dimensional, constant density,

328   steady-state shallow-water models (Chow, 2009) and two-dimensional, constant

329   density, depth-averaged, shallow-water equations (Kim et al., 2015). When a model

330   is set up for estuaries, tidal embayments, or tidal channels, the required boundary

331   conditions correspond to a time series of river discharge at the upstream boundary,

332     $Q(t)$, and a time series of water level, $H(t)$, at the downstream boundary. The

333   upstream and downstream boundaries of the modeled spatial domain are generally

334   placed adequately apart that compounding effects are avoided. This is not, however,

335   always possible in practice because tide gauges may be located within estuaries. As

336   an aside, we note that two-dimensional models require a spatial distribution of

337   boundary forcing and in practice, hydrodynamic models include methods to

338   distribute the total volumetric flow rate, $Q(t)$, across the inflow boundary while the

339   water level, $H(t)$, is typically assumed to be uniform across the outflow boundary.

340   Estuaries may also experience water level variability from internal forcing by winds

341   and waves, and accounting for these effects is outside the scope of this study.

342   However, the role of regional winds, waves, atmospheric pressure on water levels is

343   captured by this approach based on the measurement of water levels at the tide

344   gauge which are the basis as input for bivariate flood hazard assessment.

345

346   2.3.1   1D Steady State Modeling

347   One-dimensional (1D) steady state modeling of coastal flood hazards is

348   useful as a first approximation of flood hazard levels along tidal channels and

349 estuaries and can be done quickly with low computational effort. Application of 1D

350 analysis at several sites is performed to study how differences in the selection

351 process for $(\hat{Q}_T, \hat{H}_T)$ pairs can affect the estimation of flood hazard levels. Flood

352 hazard levels are computed by solving the gradually varied flow equation under the

353 assumption of a rectangular channel with spatially variable Manning n_m, width w,

354 and depth h as follows (Chow, 2009)

355
$$\frac{\mathrm{d}\eta}{\mathrm{d}x} = -\frac{S_f}{1-Fr^2} \qquad [3]$$

356 where x represents distance measured inland from the mouth of the estuary,

357 $Fr=Q/(gh^3w^2)^{1/2}$ is the Froude Number and $S_f= (n_m\,Q/w)^2/h^{10/3}$ represents the

358 friction slope. Eq. [3] is integrated with geometrical data for each site, n_m=0.032 m-

359 $^{1/3}$s, the downstream water level boundary given by $\hat{H}$, and a river discharge given

360 by $\hat{Q}$. Numerical integration is performed with the 4th/5th order Runge Kutta Scheme

361 ode45 supported by Matlab (Mathworks, Natick, MA). We note that the relatively

362 simple channel geometry and resistance approximation is used herein to examine

363 the relative differences between profiles from Scenarios S1-S4, and not to estimate

364 flood hazard along these rivers in an absolute sense. More detailed geometry and

365 resistance modeling will change the absolute value of flood hazard heights, but have

366 little impact on the relative difference between scenarios.

367

368   2.3.2 2D Unsteady Modeling

369   Two-dimensional (2D) unsteady modeling is performed at one of the four

370 sites, Newport Bay, to characterize limitations of the 1D steady state approximation

371 and to study how the relative timing of the flood peak and high tide level can affect

372 the flood hazard characterization. The 2D model BreZo (Begnudelli et al., 2008; Kim

373 et al., 2015) is applied based on a previous validation at Newport Bay (Gallien et al.,

374 2014, 2011). BreZo relies on an unstructured mesh of triangular elements with

375 varying size to capture the Bay's topography and bathymetry. The model was

16

376   originally setup to predict flood impacts in the urbanized portions of the Newport

377   Bay (City of Newport Beach, California, 2008). It features a fine resolution mesh

378   with 3 m average linear resolution cells across streets and land parcels, while across

379   the upper Newport Bay the average linear cell resolution is approximately 15 m.

380   The boundary conditions in BreZo are setup to specify the riverine discharge $\hat{Q}$

381   entering the upper Newport Bay at the outlet of the San Diego Creek, while water

382   level $\hat{H}$ is specified along a boundary placed a short distance offshore of the

383   embayment.

384   For unsteady analysis, riverine discharge entering Newport Bay was

385   modeled with a triangular hydrograph with a peak value given by $\hat{Q}$ and a time of

386   rise and total flood duration set to 3 and 8 hours, respectively, based on analysis of

387   instantaneous discharge measurements. Additionally, ocean water level changes

388   were modeled using a sinusoidal function with a 12 hour period (based on

389   semidiurnal tides) such that the maximum ocean water level equals $\hat{H}$. These

390   approximations followed preliminary modeling, which demonstrated that flood

391   heights in the upper bay were much more sensitive to the magnitude of the peak

392   flow than the duration of the event, within the range of observed values, and that

393   high-water levels were not sensitive to the precise shape of the tidal forcing. We

394   note that this may not be true in all systems, and thus these approximations are not

395   presented as a generalization but rather as a reasonable simplification given specific

396   site conditions.

397   Figure 4 presents the sinusoidal ocean forcing and the triangular inflow

398   hydrograph. To report the sensitivity of maximum water levels to the relative timing

399   of the peak inflow and peak high tide, the "OR" Hazard Scenario was repeated using

400   an inflow hydrograph that was shifted forward and backwater by as much as 6

401   hours, as shown in Figure 4.
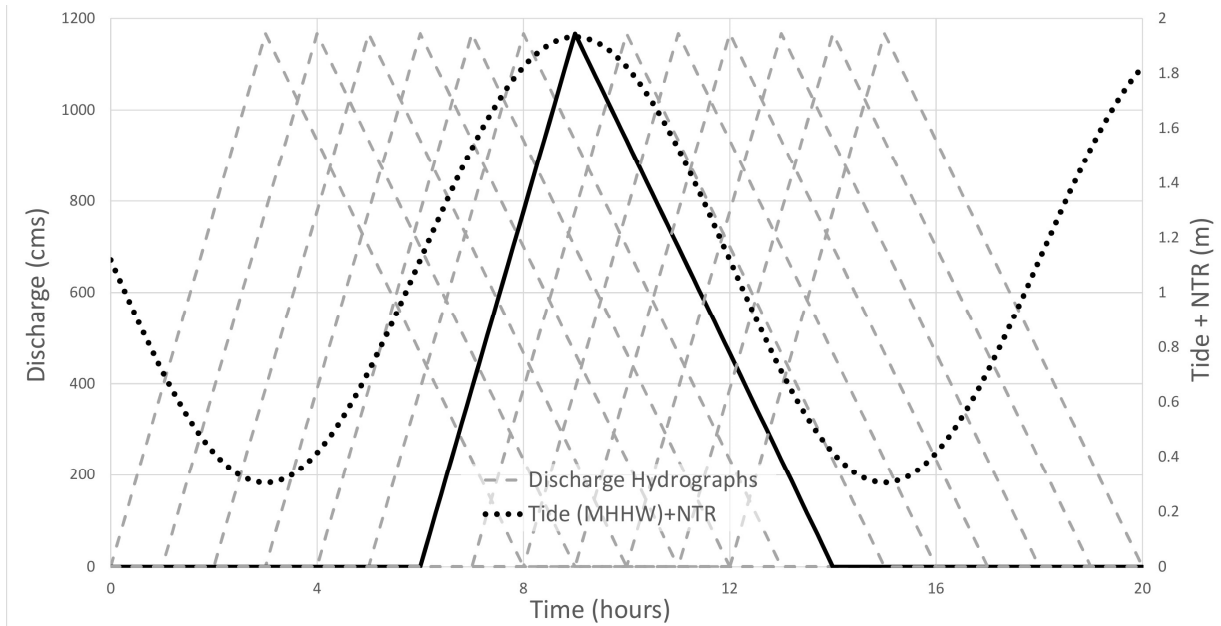
Figure 4: Inflow into Newport Bay was modeled with a triangular hydrograph with a duration and time to rise specified based on historical average values, and the ocean water level was modeled with a sinusoidal function with a period of 12 hours based on semidiurnal tides. The sensitivity of water level predictions to the time lag between peak river flow and high tide was examined with additional simulations involving forward and backwards time lags up to 6 hours.

All modeling results are expressed in metric units and referenced to the NAD83 State Plane horizontal coordinate system and NAVD88 vertical datum.

3. Results

3.1 Bivariate Statistical Analysis

Correlation analysis between $\hat{Q}$ and $\hat{H}$ defined by TWL revealed no statistical significance at these southern California sites due to relatively small storm surges compared to variability in high tide levels attributed to astronomical factors. However, correlation was found using NTR as a surrogate for $\hat{H}$ at three of the four sites considered: LAR, SAR and NB.

Kendall tau and Spearman rho correlation coefficients between variables $\hat{Q}$ and $\hat{H}$ (defined using NTR) are presented in Table 1 along with p-values. A p-value of less than 0.05 suggests a correlation at 5% significance level. We apply the

421 method of Sadegh et al. (2018) to find the distribution functions that best describe

422 the univariate distribution of river flow and NTR. Additionally, the JOE bivariate

423 Copula function was then found to best describe the correlation structure between

424 $\hat{Q}$ and $\hat{H}$ in all sites, given the marginal probabilities as shown in Fig. 3.

425

Site	Kendall		Spearman		Pearson		Distribution	
	Correlation Coefficient	p-value	Correlation Coefficient	p-value	Correlation Coefficient	p-value	Q	H
LAR	0.2616	0.0167	0.3880	0.0122	0.4666	0.0021	rayleigh	logistic
SAR	0.3357	0.0012	0.4907	0.0006	0.4303	0.0032	nakagami	logistic
NB	0.3229	0.0113	0.4478	0.0115	0.5659	0.0009	inverse gaussian	logistic

426 **Table 1:** Correlation coefficients between variables $\hat{Q}$ and $\hat{H}$.

427

Site	S1: Marginal Q		S2: Marginal H		S3: AND		S4: OR	
	$\hat{Q}$	$\hat{H}$	$\hat{Q}$	$\hat{H}$	$\hat{Q}$	$\hat{H}$	$\hat{Q}$	$\hat{H}$
LAR	2435	1.611	10	1.901	2295	1.882	2531	1.914
SAR	693	1.611	10	1.983	640	1.965	730	1.997
NB	1090	1.611	10	1.922	1005	1.911	1167	1.930

428 **Table 2:** Scenario S1-S4 values of the 50-year return period river discharge (m³/s) and ocean level (m above

429 NAVD88) resulting from bivariate analysis as shown in Figure 3. Note that the AND and OR values correspond

430 to maximum probability density (or likelihood).

431   Flood hazard levels $\hat{Q}$ and $\hat{H}$ for T=50 year resulting from the method of

432 Sadegh et al. (2018) for Scenarios S1-S4 are presented in Table 2. Note that the

433 "Marginal Q" scenarios all use a downstream water level corresponding to mean

434 higher high water, and all of the "Marginal H" scenarios use a small (relative to the

435 extreme flows) river discharge ($\sim$ average daily flow) taken as 10 m³/s. These

436 results show that the LAR has larger river discharge values than SAR and NB, yet

437 somewhat surprisingly, NB has larger river discharge values than SAR despite a

438 much smaller watershed area. This is attributed to control of runoff by dams. Also,

439 note that the water level of the "Marginal H" scenario differs between the three sites

19

440   despite all three relying on the Los Angeles Tide gauge. This is attributed to

441   differences in the record length arising from joint probability analysis of tide gauge

442   data and river gauge data.

443

444   3.2 1D Flood Hazard Analysis

445   1D steady state water surface profiles were computed for the 12 sets of

446    $(\hat{Q}_T, \hat{H}_T)$ pairs presented in Table 2 corresponding to S1-S4 at LAR, SAR and NB and

447   are presented in Figure 5a, c, and e, respectively. Focusing first on the "Marginal H"

448   and "Marginal Q" scenarios, these results shows that there is a transition in the

449   dominant factor controlling flood hazard levels along the length of the system with

450   H controlling flood hazards near the outlet and Q controlling flood hazards further

451   inland. The length of oceanic control is relatively long for NB (~4 km) and LAR (~2

452   km) and relatively short SAR (~ 300 m). Water levels from the "AND" scenario are

453   lower than the higher of the two marginal scenarios at inflow and outflow

454   boundaries, but, higher within an interior region where the marginal profiles

455   intersect. On the other hand, the "OR" scenario yields a water surface profile that is

456   always above both marginal scenario profiles. Conceptually, these results show that

457   the "OR" scenario represents a more conservative (i.e., cautious) representation of

458   the spatially variable water surface profile associated with return period T than the

459   "AND" scenario which is expected based on the magnitude of the boundary forcing

460   (see Table 2).

461   FEMA (2015) guidance recommends mapping of flood hazard levels in tidally

462   affected reaches based on the pointwise maximum of the two marginal scenarios.

463   This profile (labeled "FEMA") is presented in Figure 5b, d, and f for LAR, SAR and

464   NB, respectively, alongside the "AND", "OR", and a proposed composite profile based

465   on the pointwise maximum of the "H Marginal", "Q Marginal" and "AND" hazard

466   scenarios. At all three sites, the FEMA method underestimates the T year return

467   period water level, compared to the "AND" scenario, within a region where the

468   marginal water surface profiles intersect. Hence, the proposed composite profile is
469   slightly higher than the FEMA method profile where there are physical
470   compounding effects due to the interaction of river and oceanic influences on water
471   levels; otherwise the proposed composite profile tracks the FEMA method profile.

472
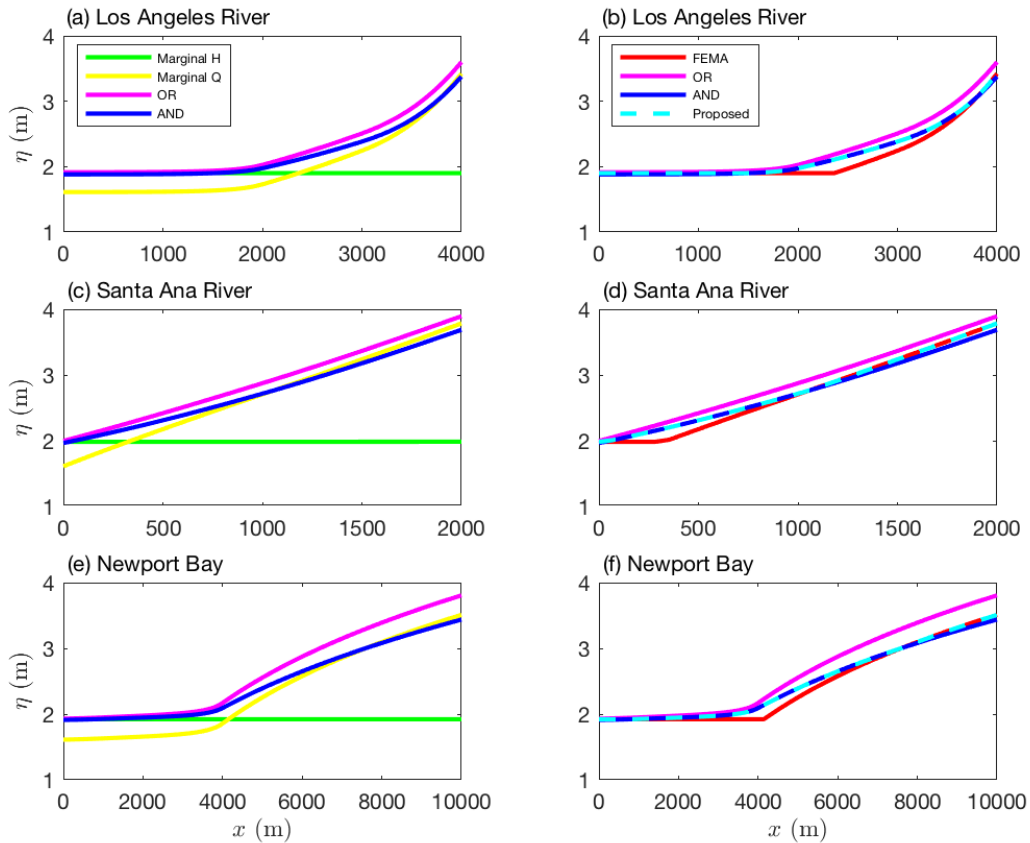
Figure 5: Steady state water surface profiles versus distance from mouth, x, based on "Marginal H", "Marginal Q", "OR" and "AND" scenarios for (a) LAR, (c) SAR and (e) NB. Composite profiles based on the FEMA methodology and a proposed extension that considers the "Most Likely AND" scenario for (b) LAR, (d) SAR and (f) NB.

477

478   3.3 2D Flood Hazard Analysis

479   Two-dimensional modeling of flood hazards in Newport Bay leads to spatially
480   and temporally distributed water levels. Hence, flood hazards are mapped based on
481   the point maximum water level attained over an unsteady simulation covering the

482   rise and fall of a flood peak with magnitude $\hat{Q}$ and the rise and fall of an ocean tide of

483   height $\hat{H}$. Results are presented first for the case of the temporal coincidence in the

484   two peaks, and later the sensitivity of the results to the time lag between peaks is

485   shown.

486
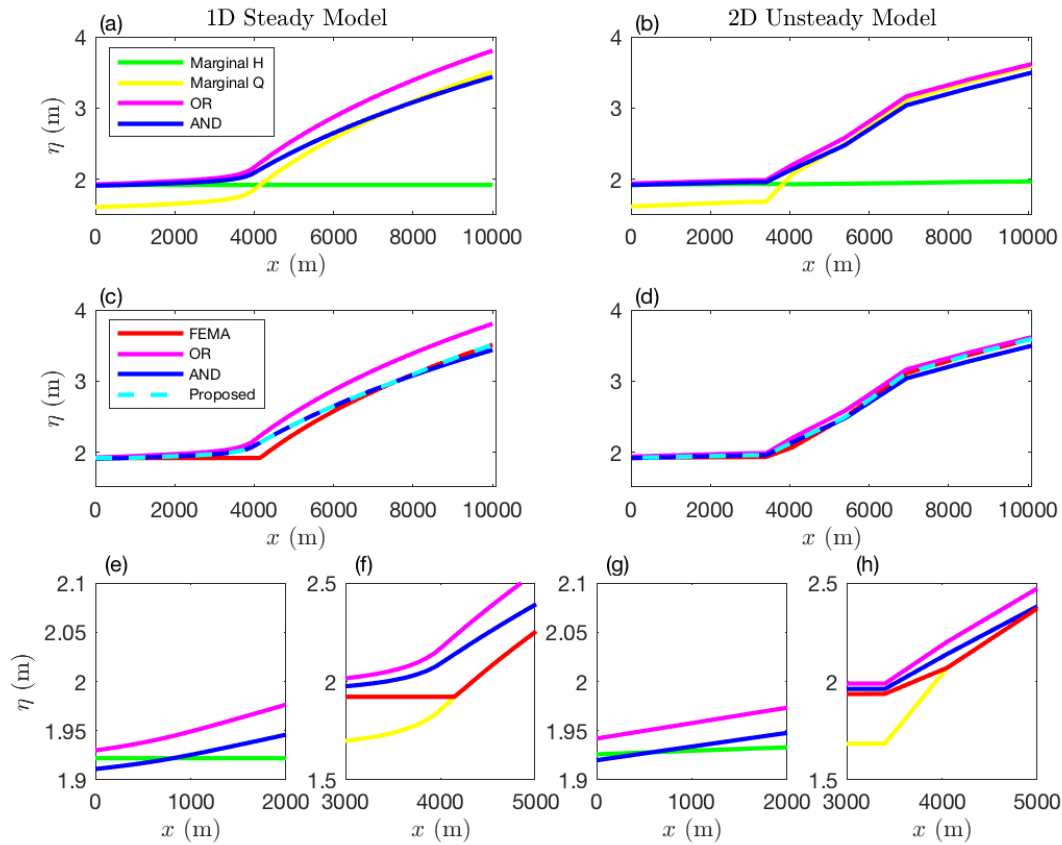
Figure 6: NB flood hazard levels versus distance from mouth, x, based on 1D steady model (a,c,e,f) and 2D

unsteady model (b,d,g,h). 2D results based on 5 points selected from along the main channel and linearly

interpolated between points. Using both 1D and 2D approaches, the "AND" scenario predicts lower flood

hazard levels compared to the maximum of the marginal profiles at the mouth (x=0) and head (x=10000 m),

and higher flood hazard levels near where the marginal profiles intersect (x=4000 m).; the "OR" scenario

predicts the highest water levels everywhere. Differences between 1D and 2D models attributed to

unsteadiness and treatment of complex geometry.

494

495   A comparison of extreme water level scenarios (S1-S4) along the main

496   channel of Newport bay using 1D and 2D methods is shown in Figure 6. For each

497 scenario, the modeling method has little impact on water profiles in the lower bay (x

498 < 4000 m) while differences are evident in upper bay (x > 4000 m) and attributed

499 mainly to differences in the treatment of complex system topography/bathymetry.

500 That is, the 1D model assumes a rectangular cross-sectional with a width and depth

501 based on the main channel, while the 2D model resolves both channel and

502 floodplain/marsh topography allowing for greater conveyance at higher flood

503 stages. Similar to the 1D model results presented earlier, the 2D results show that

504 the "AND" scenario predicts lower flood hazard levels compared to the maximum of

505 the marginal profiles at the mouth (x=0) and head (x =10000 m), and higher flood

506 hazard levels near where the marginal profiles intersect (x =4000 m). Additionally,

507 the "OR" scenario predicts the highest water levels everywhere. A magnified view of

508 water surface profiles at the mouth is presented in Fig. 6e (1D) and 6g (2D) and at x

509 =4000 m in Fig. 6f (1D) and 6h (2D).

510 Figure 6 also shows the FEMA (2015) composite profile and the proposed

511 composite water surface profile, which takes the pointwise maximum of the

512 marginal scenarios and the "AND" scenario. In this case, the 2D modeling predicts a

513 smaller difference between composite profiles (~6 cm) than 1D modeling (~15 cm)

514 and this is attributed mainly to the treatment of complex topography. Nevertheless,

515 small height differences can be significant with respect to the delineation of flood

516 hazard zones where floodplain topography is relatively flat. For example, a vertical

517 height of 6 cm on a slope of 1/1000 implies a 60 m change in horizontal position

518 which is larger than many land parcels in developed areas.

519 Figure 7a shows the spatial distribution of the differences between water

520 surface levels based on the FEMA method and the proposed method. The largest

521 differences ($d\eta$ ≥1 cm) are found in the lower NB and are maximum at the

522 constriction between upper and lower bay located at Pacific Coast Highway. Figure

523 7a also shows differences in the western part of NB, off line from the main channel

524 connecting San Diego Creek to the mouth of NB ,
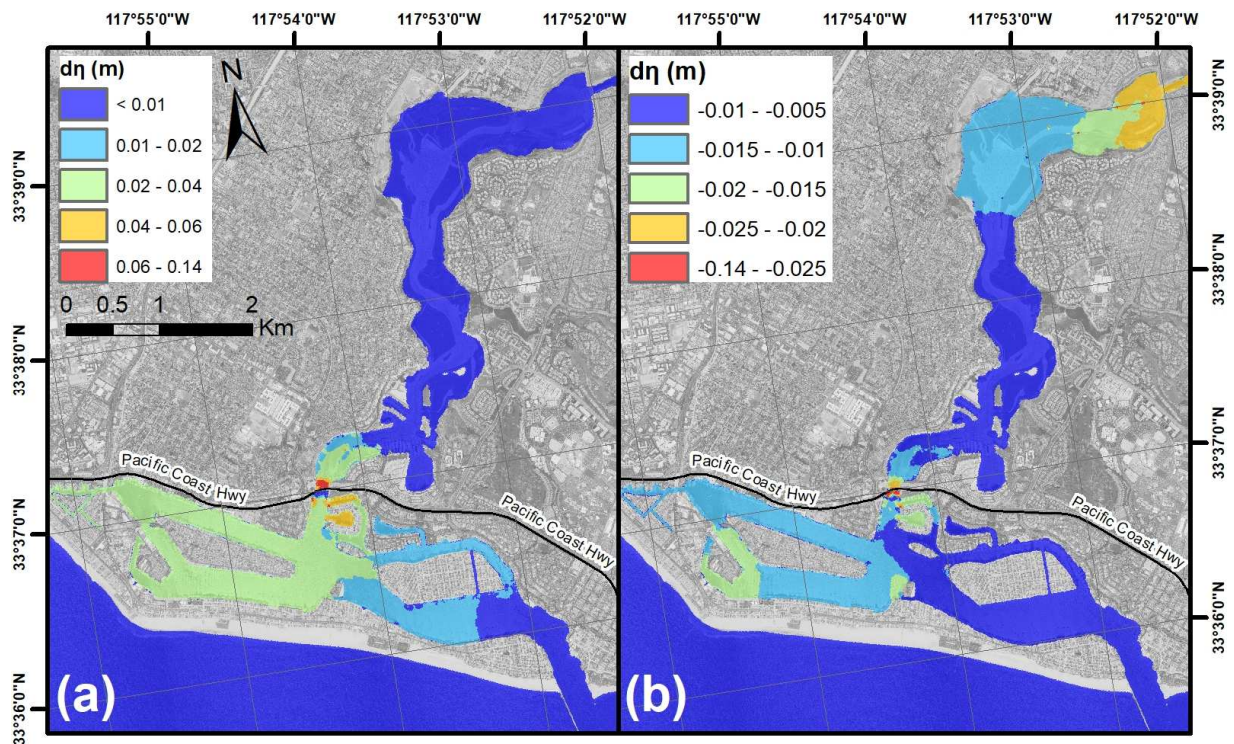
Figure 7: Difference in water surface elevations between (a) the proposed composite profile and the FEMA composite profile, and (b) "OR Hazard" scenarios with coincident peaks at hour 9 vs scenarios with shifted peaks that achieve maximum water surface level.

The effect of the relative timing of peak inflow and high tide to achieve maximum water surface elevations using the "OR" Hazard scenario was found to be relatively small compared to differences between hazard scenarios (i.e., AND vs. OR). Figure 7b shows color contours of the difference in water surface elevations between the scenario where hydrograph peaks are matched in time (peak at time=9 hours in Figure 4) and water surface elevations obtained by shifting the peaks in time to achieve maximum water level. In the uppermost section of the upper bay maximum water level is achieved by delaying peak river discharge by one hour (peak Q at hour 10 in Figure 4), while in the lower bay maximum water level is achieved by advancing peak Q by one hour (peak Q at hour 8 in Figure 4). The difference between water levels based on the timing of high tides vs peak flow was found to be less than 3 cm across the majority of the bay. This constitutes only about a third of the difference between the proposed composite profile and the FEMA

542　(2015) composite profile. This result provides *a posteriori* validation of selecting Q

543　and H as the basis for bivariate statistical analysis at this site as opposed to other

544　system attributes such as the time lag between river flow and high tide.

545

546　**4. Discussion**

547　　　Multivariate statistical analysis is limited here to two variables (bivariate

548　analysis) chosen to represent annual maximum river discharge and ocean level.

549　Hazard scenarios beyond two variables are possible using copula-based methods,

550　however expansion to higher dimensions can have drawbacks including uncertainty

551　bounds so large that no conclusion may be drawn from its results (see Bevacqua et

552　al. (2017) for example). For the sites considered, the importance of the randomness

553　of annual maximum river discharge and ocean level (over other variables) justifies

554　the formulation of the bivariate statistical analysis problem around these two

555　variables. In systems where flood hazards are controlled by randomness in other

556　factors such as waves or rainfall or even uncertain internal processes, a different

557　approach would be needed. Examples of internal processes include the frictional

558　interaction between streamflow and tidal levels (Kukulka and Jay, 2003a, 2003b;

559　Moftakhari et al., 2013, 2016). Applications at a broader set of sites are warranted to

560　better understand the broader applicability of the proposed method of bivariate

561　analysis for flood hazard assessment in tidal channels and estuaries.

562　　　Composite profiles derived from the pointwise maximum of water levels

563　predicted by two or more hydrodynamic modeling scenarios offer a practical

564　approach for delineating compound flood hazards in tidal channels and estuaries for

565　a return period, *T*. Only a limited number of (relatively expensive) hydrodynamic

566　model simulations need to be completed despite an infinite number of possible

567　forcing scenarios based on bivariate statistical analysis. The most likely "AND

568　Hazard" was identified as a promising candidate for extending FEMA (2015)

569　guidance on flood hazard mapping in tidal channels and estuaries to improve

570 assessment of compound flood hazards. That is, results here suggest that the FEMA

571 (2015) may underestimate the flood hazard level over an interior section of tidal

572 reaches and estuaries where high water levels are sensitive to both riverine

573 discharge and ocean levels. In NB, this section corresponds to the urbanized lower

574 bay where exposure and vulnerability to flooding is highest. Moreover, an important

575 implication is that extreme water levels may be higher at certain points within a

576 system from combinations of river discharge and ocean heights that both fall below

577 the return levels given by the marginal distribution (i.e., univariate analysis). On the

578 other hand, the most likely "OR Hazard" scenario results in boundary forcing that

579 exceeds the return levels given by univariate analysis, and it produces water levels

580 that are higher than the marginal scenarios and the "AND Hazard" scenario. The "OR

581 Hazard" scenario could be useful when there is interest in using a single

582 hydrodynamic modeling scenario to represent compound flood hazard levels and to

583 avoid the need to compute composite profiles from multiple hydrodynamic

584 modeling scenarios. Importantly, the "OR Hazard" represents a more conservative

585 interpretation of the T year return period hazard compared to traditional univariate

586 assessment methods as well the "AND Hazard" scenario.

587 This paper points to the possibility of more robust framework for mapping

588 coastal flood hazards in tidal channels in estuaries that takes advantage of recent

589 advances in multivariate statistical modeling (e.g., Sadegh et al. 2018) and

590 hydrodynamic coastal flood hazard mapping (e.g., Gallien et al. 2011, Luke et al.

591 2018) and is in line with the limited resources and past practices of flood hazard

592 mapping (Burby 2001, FEMA 2015). In short, the method involves: (1) bivariate

593 statistical analysis where correlations in extreme values exist, (2) selection of a

594 limited number of $\hat{Q}$ / $\hat{H}$ pairs for return period T, (3) hydrodynamic modeling of

595 the chosen pairs to produce extreme water levels, and (4) synthesis of the model

596 results to provide a spatial distribution of water level associated with return period

597 T. If this approach is taken to be more robust than existing methods (and more

598 research will be needed at a broader set of sites to make this assessment), then the
599 limited testing presented herein points to existence of compound flood hazards that
600 are presently underestimated by the existing FEMA method for tidal channels
601 (FEMA 2015). That is, at all three sites, there was a reach of the channel where the
602 proposed composite profile accounting for the "AND Hazard" scenario was higher
603 than the composite profile accounting only for marginal scenarios as a result of
604 physical compounding effects. Recent research has also shown that flood hazard
605 zones in the U.S. are underestimated due to poor representation of pluvial flood
606 hazards (e.g., Wing et al. 2017).

607   Finally, we note that the hydrodynamic modeling shown here for Newport
608 Bay is for only a single return period to demonstrate the hybrid statistical-
609 hydrodynamic framework. To consider other return periods, the corresponding iso-
610 probability curve (e.g., Figure 3) needs to be selected to define the preferred
611 scenario.

612

613   **5. Conclusions**

614   A method of linking statistical analysis with hydrodynamic modeling to map
615 compounds in tidal channels and estuaries is presented for cases where flood
616 hazards are associated with both high river discharge (upstream forcing) and high
617 ocean levels (downstream forcing). Bivariate statistical analysis is introduced to
618 create combinations of river discharge and ocean levels suited for hydrodynamic
619 modeling, and extreme water levels produced by hydrodynamic models are
620 synthesized to create a composite water surface profile representative of return
621 period, T. The method accounts for compound flood hazards in two ways. First, it
622 accounts for statistical correlation between upstream and downstream forcing
623 which represents one dimension of compound hazards. Secondly, hydrodynamic
624 modeling accounts for physical compounding effects. Importantly, this work shows
625 that water levels at interior points of a tidal channel or estuary resulting from the

626 bivariate "AND" hazard scenario can be higher than water levels from marginal

627 scenarios even though the boundary forcing is smaller than the corresponding

628 marginal scenarios. This is attributed to physical compounding effects, i.e., nonlinear

629 interactions between discharge and water level described by shallow-water wave

630 theory. This work also shows that if a single scenario is needed to depict spatially

631 distributed compound flood hazard levels, the bivariate "OR" hazard can be used

632 and results here show that it provides a conservative assessment of the T year

633 return period hazard.

634

635 **Acknowledgments**

640

641 **References:**

642 Begnudelli, L., Sanders, B.F., Bradford, S.F., 2008. Adaptive Godunov-Based Model for Flood Simulation.
643   J. Hydraul. Eng. 134, 714–725. https://doi.org/10.1061/(ASCE)0733-9429(2008)134:6(714)
644 Burby, R.J., 2001. Flood insurance and floodplain management: the US experience. Environ. Hazards 3,
645   111–122. https://doi.org/10.3763/ehaz.2001.0310
646 Chow, V.T., 2009. Open-channel hydraulics. Blackburn Press, Caldwell, NJ.
647 City of Newport Beach, California, 2008. Vulnerability of the Newport Harbor Area to Flooding by
648   Extreme Tides.
649 Coles, S.G., Heffernan, J., Tawn, J., 1999. Dependence Measures for Extreme Value Analyses. Extremes 2,
650   339–365. https://doi.org/10.1023/A:1009963131610
651 Dasgupta, S., Laplante, B., Murray, S., Wheeler, D., 2011. Exposure of developing countries to sea-level
652   rise and storm surges. Clim. Change 106, 567–579. https://doi.org/10.1007/s10584-010-9959-6
653 FEMA, 2018. Guidelines and Standards for Flood Risk Analysis and Mapping [WWW Document]. URL
654   https://www.fema.gov/guidelines-and-standards-flood-risk-analysis-and-mapping (accessed
655   5.2.18).
656 FEMA, 2015. Guidance for flood risk analysis and mapping; combined coastal and riverine floodplain
657   (No. Guidance Document 32). FEMA.
658 Friedrichs, C.T., 2010. Barotropic tides in channelized estuaries, in: Valle-Levinson, A. (Ed.),
659   Contemporary Issues in Estuarine Physics. Cambridge University Press, Cambridge, pp. 27–61.
660   https://doi.org/10.1017/CBO9780511676567.004

661 Gallien, T., Kalligeris, N., Delisle, M.-P., Tang, B.-X., Lucey, J., Winters, M., 2018. Coastal Flood Modeling
662   Challenges in Defended Urban Backshores. Geosciences 8, 450.
663   https://doi.org/10.3390/geosciences8120450
664 Gallien, T.W., Sanders, B.F., Flick, R.E., 2014. Urban coastal flood prediction: Integrating wave
665   overtopping, flood defenses and drainage. Coast. Eng. 91, 18–28.
666   https://doi.org/10.1016/j.coastaleng.2014.04.007
667 Gallien, T.W., Schubert, J.E., Sanders, B.F., 2011. Predicting tidal flooding of urbanized embayments: A
668   modeling framework and data requirements. Coast. Eng. 58, 567–577.
669   https://doi.org/10.1016/j.coastaleng.2011.01.011
670 Genest, C., Favre, A.-C., 2007. Everything You Always Wanted to Know about Copula Modeling but Were
671   Afraid to Ask. J. Hydrol. Eng. 12, 347–368. https://doi.org/10.1061/(ASCE)1084-
672   0699(2007)12:4(347)
673 Geyer, W.R., 2010. Estuarine salinity structure and circulation, in: Valle-Levinson, A. (Ed.), Contemporary
674   Issues in Estuarine Physics. Cambridge University Press, Cambridge, pp. 12–26.
675   https://doi.org/10.1017/CBO9780511676567.003
676 Hallegatte, S., Green, C., Nicholls, R.J., Corfee-Morlot, J., 2013. Future flood losses in major coastal cities.
677   Nat. Clim. Change 3, 802–806. https://doi.org/10.1038/nclimate1979
678 Hanson, S., Nicholls, R., Ranger, N., Hallegatte, S., Corfee-Morlot, J., Herweijer, C., Chateau, J., 2011. A
679   global ranking of port cities with high exposure to climate extremes. Clim. Change 104, 89–111.
680   https://doi.org/10.1007/s10584-010-9977-4
681 Hao, Z., Singh, V.P., 2016. Review of dependence modeling in hydrology and water resources. Prog.
682   Phys. Geogr. 40, 549–578. https://doi.org/10.1177/0309133316632460
683 Hawkes, P.J., 2006. Use of Joint Probability Methods in Flood Management: A Guide to Best Practice
684   (R&D Technical Report No. FD2308/TR2). DEFRA.
685 Hawkes, P.J., Gouldby, B.P., Tawn, J.A., Owen, M.W., 2002. The joint probability of waves and water
686   levels in coastal engineering design. J. Hydraul. Res. 40, 241–251.
687   https://doi.org/10.1080/00221680209499940
688 Heffernan, J.E., Tawn, J.A., 2004. A conditional approach for multivariate extreme values (with
689   discussion). J. R. Stat. Soc. Ser. B Stat. Methodol. 66, 497–546. https://doi.org/10.1111/j.1467-
690   9868.2004.02050.x
691 Hillier, J.K., Macdonald, N., Leckebusch, G.C. and Stavrinides, A., 2015. Interactions between apparently
692   'primary' weather-driven hazards and their cost. Environmental Research Letters, 10(10),
693   p.104003.
694 Hinkel, J., Lincke, D., Vafeidis, A.T., Perrette, M., Nicholls, R.J., Tol, R.S.J., Marzeion, B., Fettweis, X.,
695   Ionescu, C., Levermann, A., 2014. Coastal flood damage and adaptation costs under 21st century
696   sea-level rise. Proc. Natl. Acad. Sci. 111, 3292–3297. https://doi.org/10.1073/pnas.1222469111
697 Hinkel, J., Nicholls, R.J., Vafeidis, A.T., Tol, R.S.J., Avagianou, T., 2010. Assessing risk of and adaptation to
698   sea-level rise in the European Union: an application of DIVA. Mitig. Adapt. Strateg. Glob. Change
699   15, 703–719. https://doi.org/10.1007/s11027-010-9237-y
700 Hoitink, A.J.F., Jay, D.A., 2016. Tidal river dynamics: Implications for deltas. Rev. Geophys. 54, 240–272.
701   https://doi.org/10.1002/2015RG000507
702 Jay, D.A., 2010. Estuarine variability, in: Valle-Levinson, A. (Ed.), Contemporary Issues in Estuarine
703   Physics. Cambridge University Press, Cambridge, pp. 62–99.
704   https://doi.org/10.1017/CBO9780511676567.005
705 Kappes, M.S., Keiler, M., von Elverfeldt, K. and Glade, T., 2012. Challenges of analyzing multi-hazard risk:
706   a review. Natural hazards, 64(2), pp.1925-1958.
707 Kennish, M.J. (Ed.), 2004. Estuarine research, monitoring, and resource protection, Marine science
708   series. CRC Press, Boca Raton, Fla.

709   Kim, B., Sanders, B.F., Famiglietti, J.S., Guinot, V., 2015. Urban flood modeling with porous shallow-
710   water equations: A case study of model errors in the presence of anisotropic porosity. J. Hydrol.
711   523, 680–692. https://doi.org/10.1016/j.jhydrol.2015.01.059
712   Kukulka, T., Jay, D.A., 2003a. Impacts of Columbia River discharge on salmonid habitat: 1. A
713   nonstationary fluvial tide model. J. Geophys. Res. 108.
714   Kukulka, T., Jay, D.A., 2003b. Impacts of Columbia River discharge on salmonid habitat: 2. Changes in
715   shallow-water habitat. J. Geophys. Res. 108.
716   Lanzoni, S., Seminara, G., 1998. On tide propagation in convergent estuaries. J. Geophys. Res. Oceans
717   103, 30793–30812. https://doi.org/10.1029/1998JC900015
718   Leonard, M., Westra, S., Phatak, A., Lambert, M., van den Hurk, B., McInnes, K., Risbey, J., Schuster, S.,
719   Jakob, D., Stafford-Smith, M., 2014. A compound event framework for understanding extreme
720   impacts. Wiley Interdiscip. Rev. Clim. Change 5, 113–128. https://doi.org/10.1002/wcc.252
721   Luke, A., Sanders, B.F., Goodrich, K.A., Feldman, D.L., Boudreau, D., Eguiarte, A., Serrano, K., Reyes, A.,
722   Schubert, J.E., AghaKouchak, A. and Basolo, V., 2018. Going beyond the flood insurance rate
723   map: insights from flood hazard map co-production. *Natural Hazards and Earth System*
724   *Sciences*, *18*(4), pp.1097-1120.
725   Moftakhari, H.R., Jay, D.A., Talke, S.A., 2016. Estimating river discharge using multiple-tide gauges
726   distributed along a channel. J. Geophys. Res. Oceans 121, 2078–2097.
727   https://doi.org/10.1002/2015JC010983
728   Moftakhari, H.R., Jay, D.A., Talke, S.A., Kukulka, T., Bromirski, P.D., 2013. A novel approach to flow
729   estimation in tidal rivers. Water Resour. Res. 49, 4817–4832.
730   https://doi.org/10.1002/wrcr.20363
731   Moftakhari, Salvadori, G., AghaKouchak, A., Sanders, B.F., Matthew, R.A., 2017. Compounding effects of
732   sea level rise and fluvial flooding. Proc. Natl. Acad. Sci. 114, 9785–9790.
733   https://doi.org/10.1073/pnas.1620325114
734   Monismith, S.G., 2010. Mixing in estuaries, in: Valle-Levinson, A. (Ed.), Contemporary Issues in Estuarine
735   Physics. Cambridge University Press, Cambridge, pp. 145–185.
736   https://doi.org/10.1017/CBO9780511676567.008
737   Neal, J., Keef, C., Bates, P., Beven, K., Leedal, D., 2013. Probabilistic flood risk mapping including spatial
738   dependence. Hydrol. Process. 27, 1349–1363. https://doi.org/10.1002/hyp.9572
739   Purvis, M.J., Bates, P.D., Hayes, C.M., 2008. A probabilistic methodology to estimate future coastal flood
740   risk due to sea level rise. Coast. Eng. 55, 1062–1073.
741   https://doi.org/10.1016/j.coastaleng.2008.04.008
742   Ross, D.A., 1995. Introduction to oceanography. HarperCollinsCollegePublishers, New York, NY.
743   Sadegh, M., Moftakhari, H., Gupta, H.V., Ragno, E., Mazdiyasni, O., Sanders, B., Matthew, R.,
744   AghaKouchak, A., 2018. Multi-hazard scenarios for analysis of compound extreme events.
745   Geophys. Res. Lett. https://doi.org/10.1029/2018GL077317
746   Sadegh, M., Ragno, E., AghaKouchak, A., 2017. Multivariate Copula Analysis Toolbox (MvCAT):
747   Describing dependence and underlying uncertainty using a Bayesian framework: MvCAT. Water
748   Resour. Res. 53, 5166–5183. https://doi.org/10.1002/2016WR020242
749   Salvadori, G., De Michele, C., Kottegoda, N., Rosso, R., 2007. Extremes in nature: an approach using
750   copulas, Water science and technology library. Springer, Dordrecht.
751   Salvadori, G., Durante, F., De Michele, C., Bernardi, M., Petrella, L., 2016. A multivariate Copula-based
752   framework for dealing with Hazard Scenarios and Failure Probabilities. Water Resour. Res. 52,
753   3701–3721. https://doi.org/10.1002/2015WR017225
754   Salvadori, G., Durante, F., Tomasicchio, G.R., D'Alessandro, F., 2015. Practical guidelines for the
755   multivariate assessment of the structural risk in coastal and off-shore engineering. Coast. Eng.
756   95, 77–83. https://doi.org/10.1016/j.coastaleng.2014.09.007

757   Sanders, B.F., 2017. Hydrodynamic Modeling of Urban Flood Flows and Disaster Risk Reduction, in:
758   Natural Hazard Science, Oxford Research Encyclopedias.
759   Sanders, B.F., Schubert, J.E., Detwiler, R.L., 2010. ParBreZo: A parallel, unstructured grid, Godunov-type,
760   shallow-water code for high-resolution flood inundation modeling at the regional scale. Adv.
761   Water Resour. 33, 1456–1467. https://doi.org/10.1016/j.advwatres.2010.07.007
762   Sayers, P., Yuanyuan, L., Galloway, G., Penning-Rowsell, E., Fuxin, S., Kang, W., Yiwei, C., Le Quesne, T.
763   (Eds.), 2013. Flood risks management: a strategic approach. Asian Development Bank,
764   Mandaluyong City, Metro Manila, Philippines.
765   Scawthorn, C., Blais, N., Seligson, H., Tate, E., Mifflin, E., Thomas, W., Murphy, J., Jones, C., 2006. HAZUS-
766   MH Flood Loss Estimation Methodology. I: Overview and Flood Hazard Characterization. Nat.
767   Hazards Rev. 7, 60–71. https://doi.org/10.1061/(ASCE)1527-6988(2006)7:2(60)
768   Sklar, A., 1959. Fonctions de répartition à n dimensions et leurs marges. Publ Inst Stat. Univ Paris 8, 229–
769   231.
770   Torresan, S., Critto, A., Rizzi, J., Marcomini, A., 2012. Assessment of coastal vulnerability to climate
771   change hazards at the regional scale: the case study of the North Adriatic Sea. Nat. Hazards
772   Earth Syst. Sci. 12, 2347–2368. https://doi.org/10.5194/nhess-12-2347-2012
773   Ward, P.J., Couasnon, A., Eilander, D., Haigh, I.D., Hendry, A., Muis, S., Veldkamp, T.I.E., Winsemius, H.C.,
774   Wahl, T., 2018. Dependence between high sea-level and high river discharge increases flood
775   hazard in global deltas and estuaries. Environ. Res. Lett. 13, 084012.
776   https://doi.org/10.1088/1748-9326/aad400
777   Zheng, F., Leonard, M., Westra, S., 2015. Application of the design variable method to estimate coastal
778   flood risk: Design variable method to estimate flood risk. J. Flood Risk Manag. 1–13.
779   https://doi.org/10.1111/jfr3.12180
780   Zscheischler, J., Westra, S., van den Hurk, B.J.J.M., Seneviratne, S.I., Ward, P.J., Pitman, A., AghaKouchak,
781   A., Bresch, D.N., Leonard, M., Wahl, T., Zhang, X., 2018. Future climate risk from compound
782   events. Nat. Clim. Change. https://doi.org/10.1038/s41558-018-0156-3
783